Toward determining the Fife similarity parameter in turbulent pipe and channel flow

By J.C. Klewicki†

This research brief describes recent progress in both the analytical and empirical determination of the Fife similarity parameter, ϕ_c, in fully developed pipe and channel flows. This parameter is central to the construction of similarity solutions for the mean velocity profile and Reynolds shear stress profiles over an interior domain, and its determination also directly specifies the value of the von Kármán constant. Analytical progress produces a solution that supports the conjecture of Klewicki et al. (2014) that $\phi_c \to \Phi$ as $\delta^+ \to \infty$, where $\Phi \simeq 1.618034$ is the golden ratio. This solution, however, proves to be nonunique. When an a priori theory-based prescription for the location of the inertial sublayer is used to specify the curve-fitting domain, the empirical evidence indicates a value of ϕ_c between 1.59 and 1.63 that becomes independent of friction Reynolds numbers greater than $10,000$.

1. Introduction

The Fife similarity parameter, ϕ, characterizes the coordinate stretching underlying the construction of similarity solutions to the mean momentum equation in turbulent wall flows. This construction is generated by determining an invariant form of the mean equation on each layer of a continuous hierarchy of scaling layers. Like the coordinate stretching found in other similarity solutions, the role of ϕ in describing the mean flow structure is central. For example, it (i) characterizes the length-scale distribution associated with the turbulent motions responsible for wall-normal momentum transport, (ii) is intrinsically related to how the mean equation embraces distance-from-the-wall scaling, and (iii) explicitly quantifies the asymptotic value of κ, the von Kármán constant (Klewicki et al. 2009; Klewicki 2021). Self-similarity in turbulent wall flows emerges as an asymptotic property, and as a result, ϕ approaches a constant, ϕ_c, on the relevant domain at high Reynolds numbers. Here use is made of the friction Reynolds number $\delta^+ \equiv \delta u_\tau/\nu$, where $u_\tau = \sqrt{\tau_w/\rho}$ is the friction velocity, $\tau_w = \mu(\mathrm{d}U/\mathrm{d}y)|_{y=0}$ is the mean wall shear stress, and $\nu = \mu/\rho$ is the kinematic viscosity; the superscript plus sign denotes inner normalization by ν and u_τ, so $y^+ = yu_\tau/\nu$. Direct integration of the invariant momentum equation leads to closed-form profile solutions for the mean velocity (U) and the Reynolds shear stress (T) over significant portions of the scaling layer hierarchy domain. This study uses the asymptotic form of the Reynolds stress solution and the properties of the scaling layer hierarchy to describe recent efforts to analytically solve for ϕ_c.

An exposition of the development and properties of the solutions for U and T on the relevant domains (Klewicki 2021) includes detailed comparisons with high-resolution channel flow simulations to test the veracity of the analytical predictions, as well as an investigation into which empirical methods are best for estimating ϕ_c. It also attempted to analytically solve for ϕ_c but ultimately failed to attain this aim. Its highly suggestive

† University of Melbourne

but incomplete analytical treatment, along with empirical evidence, did, however, support the conjecture of Klewicki et al. (2014) that as δ^+ becomes large, $\phi_c \to \Phi$, where $\Phi = (1+\sqrt{5})/2$ is the golden ratio. If that is the case, then it is also known with analytical certainty that $\kappa = \phi_c^{-2} \to \Phi^{-2} = 2/(3+\sqrt{5})$ as $\delta^+ \to \infty$.

This research brief documents the incremental progress toward an analytical solution for the asymptotic value of ϕ_c, as well as refinements in the methods to estimate ϕ_c at any given δ^+. Toward these aims, this study first concisely introduces key equations and relations. Given that they can be found in previous publications, most of the detailed mathematical steps that are needed to establish these relations are not repeated here. Instead, a descriptive narrative generally accompanies the presentation of the particular equation. These relations are then used to document the present state of affairs relative to analytically solving for ϕ_c (under the condition $\delta^+ \to \infty$). This discussion is followed by a description of recent advances in ways to better estimate ϕ_c using data from physical experiments and direct numerical simulations (DNS).

2. Construction of an invariant form of the mean momentum equation

The analysis herein considers fully developed pressure-driven incompressible turbulent flow in an infinitely wide horizontal channel of height 2δ or in a circular pipe of diameter 2δ. The direction of the main flow is x. The coordinate in the wall-normal direction is y, with its origin at the lower wall. Uppercase U denotes the time- or ensemble-averaged velocity in the x direction, and similarly, $V = 0$ is the average velocity component in y. Lowercase u and v are, respectively, the x- and y-component velocity fluctuations about the mean. Angle brackets denote time averaging. The starting point is the differential equation describing the mean balance of forces (per unit volume) in x, as found through Reynolds decomposition of the Navier–Stokes equation and averaging. The appropriately simplified form of this equation is given by

$$\rho \frac{\mathrm{d}\langle uv\rangle}{\mathrm{d}y} = -\frac{\mathrm{d}P}{\mathrm{d}x} + \mu \frac{\mathrm{d}^2 U}{\mathrm{d}y^2}, \tag{2.1}$$

for either channel or pipe flow (with $y = R - r$, where R is the pipe radius and r is the radial coordinate). Here, μ is the dynamic viscosity and ρ is the mass density. Equation (2.1) indicates that the time-averaged effect of turbulent inertia (TI) on the left is balanced by the driving mean pressure gradient force (PG) and an opposing mean viscous force (VF) on the right. The boundary conditions are no slip at the wall and $\mathrm{d}U/\mathrm{d}y = \langle uv\rangle = 0$ at the channel/pipe center. The mean velocity gradient is a continuously decreasing function of y, and from this and the boundary conditions, one can show that the Reynolds stress profile integrates to zero and has a single maximum (Fife et al. 2009).

2.1. *Salient properties of the overall force balance*

The inner-normalized form of Eq. (2.1) is given by

$$0 = \frac{\mathrm{d}^2 U^+}{\mathrm{d}y^{+2}} + \frac{\mathrm{d}T^+}{\mathrm{d}y^+} + \epsilon^2, \tag{2.2}$$

where $T^+ = -\langle uv\rangle^+$ and $\epsilon = 1/\sqrt{\delta^+}$. While Eq. (2.2) properly identifies the nonzero terms across the half-channel, not all of the terms are leading order everywhere. Empirical observations, however, allow one to determine the progression of leading balances

associated with Eq. (2.1) on the domain $0 \leq y^+ \leq \delta^+$. That is, because there are only three terms, examining the ratio of the VF to the TI term across the flow reveals the leading balance progression. Doing so indicates that there are four layers; the first layer that abuts the wall may have a width that diminishes to zero as $\delta^+ \to \infty$ (Klewicki et al. 2009; Klewicki 2021). This detail, however, is not pertinent to the present analysis.

With a knowledge of the progression of leading balances, one can analytically deduce the scaling properties of Eq. (2.2) on the associated subdomains. Such analyses have been described in detail elsewhere (Wei et al. 2005; Fife et al. 2009; Klewicki 2021). A central feature, however, is that across the third layer, where the TI term passes through zero from positive to negative, Eq. (2.2) requires a rescaling to properly reflect the change in leading-order balance from one where the TI and VF terms are dominant (layer II) to one where the TI and PG terms are dominant (layer IV). Across layer III, all three terms are leading order, and differential transformations of the form

$$\mathrm{d}y^+ = \alpha \mathrm{d}\hat{y}, \quad \mathrm{d}T^+ = \gamma \mathrm{d}\hat{T}, \quad \text{and} \quad \mathrm{d}U^+ = \mathrm{d}\hat{U} \tag{2.3}$$

allow Eq. (2.2) to be recast as

$$0 = \frac{\mathrm{d}^2\hat{U}}{\mathrm{d}\hat{y}^2} + \frac{\mathrm{d}\hat{T}}{\mathrm{d}\hat{y}} + 1, \tag{2.4}$$

where the stretching parameters α and γ are analytically determined to be ϵ^{-1} and ϵ, respectively. Figure 1 evidences the invariance of the ratio VF/TI under the coordinate stretching for y indicated by Eq. (2.3).

2.2. *The invariant form of the mean momentum equation*

Through the use of a test function (so-called adjusted Reynolds stress), one can show that the same type of balance exchange that occurs across layer III also occurs across a continuous hierarchy of scaling layers, of which layer III is one (Wei et al. 2005). As for layer III, on each of these layers Eq. (2.2) is analytically transformed into the invariant form in Eq. (2.4), but now the stretching parameters are associated with the local change in the $\mathrm{d}T^+/\mathrm{d}y^+$ profile. Effectively, this construction involves a coordinate transformation where y^+ is replaced by the characteristic scaling layer width, W^+, and the hierarchy of layers is defined over an interior domain where the $\mathrm{d}T^+/\mathrm{d}y^+$ profile is monotonically decreasing. This construction ensures that each value on the monotonic portion of the profile uniquely corresponds to a y^+ location.

By solving for the rate of change of y^+ positions along the $\mathrm{d}T^+/\mathrm{d}y^+$ profile as a function of their values, one can derive two related results. The first is the fundamental condition for asymptotically exact dynamical self-similarity on the layer hierarchy,

$$-A = \frac{\mathrm{d}^2\hat{T}}{\mathrm{d}\hat{y}^2} \to \text{constant as } \delta^+ \to \infty. \tag{2.5}$$

The second is the relationship

$$\frac{\mathrm{d}W^+}{\mathrm{d}y^+} = \frac{A}{2} = \frac{1}{\phi}, \tag{2.6}$$

which connects the variation of the layer width distribution to dynamic self-similarity and, by doing so, reveals the momentum equation–based origin of distance-from-the-wall scaling (Fife et al. 2009; Klewicki 2021).

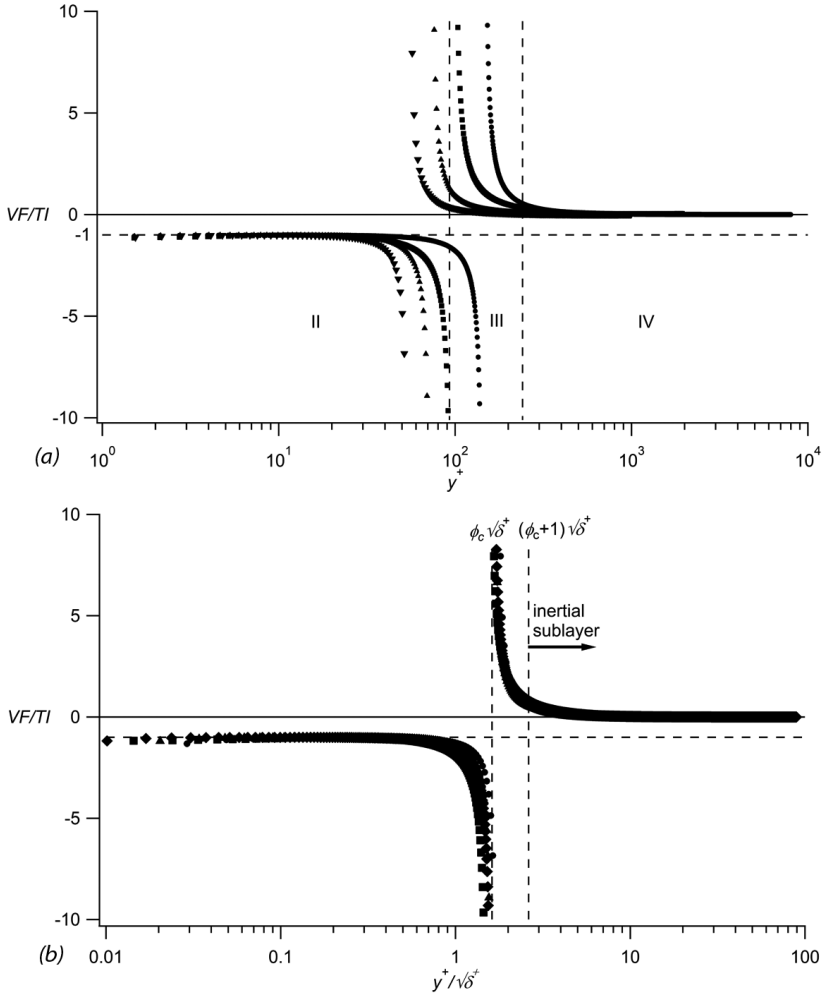

FIGURE 1. Ratio of the mean viscous force to the mean turbulent inertia in channel flow for $1000 \leq \delta^+ \leq 16,000$ (a) versus y^+ and (b) versus $y^+/\sqrt{\delta^+}$. Data are from Yamamoto & Tsuji (2018) and Kaneda & Yamamoto (2021).

Physically, Eq. (2.5) indicates that the locally normalized flux of turbulent force across an interior portion of the scaling layer hierarchy (i.e., on the inertial sublayer) asymptotically attains constancy, while Eq. (2.6) reveals that the characteristic length (scaling layer width) distribution reflects the associated linear change in the Reynolds stress profile curvature with distance from the wall.

Figure 2 shows the calculated W^+ distribution for channel flow DNS over the Reynolds number range $547 \leq \delta^+ \leq 15,994$. The slope of this profile asymptotically approaches constancy on the inertial sublayer; therefore, at any finite δ^+ the estimate of the Fife similarity parameter, ϕ, best approximates a constant value, ϕ_c. This quantity is called a similarity parameter because on the inertial sublayer $\hat{y} \rightarrow y^+/W^+ = \phi_c$ as $\delta^+ \rightarrow \infty$, which physically reflects a stretching of y with the local characteristic length of

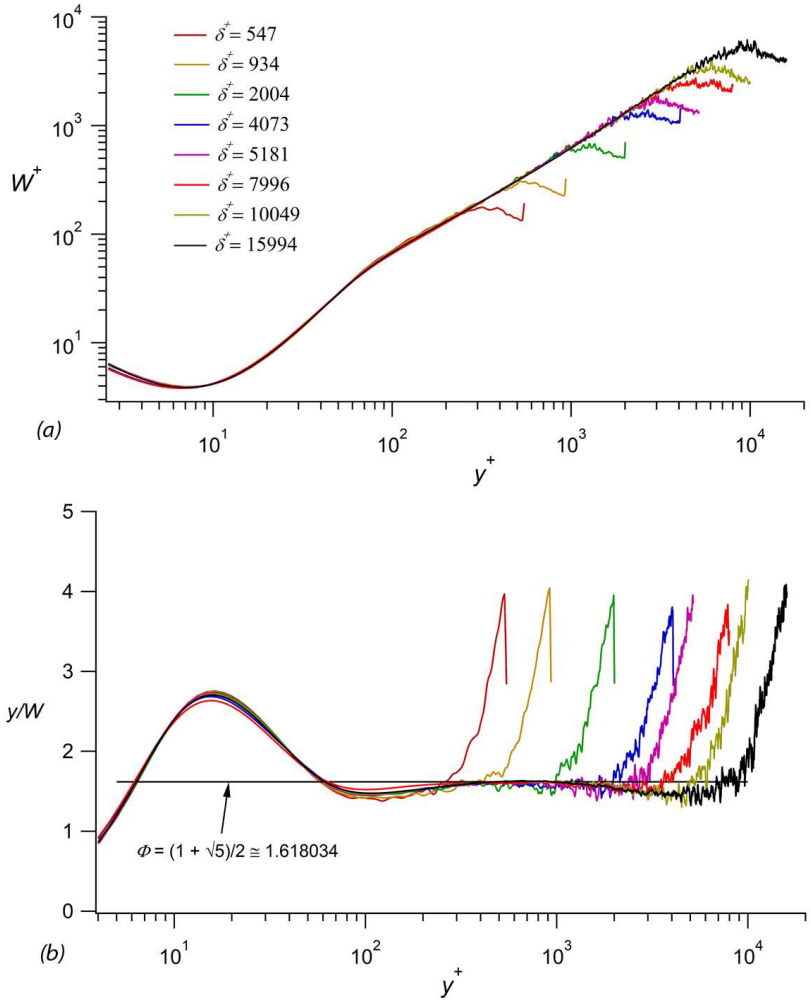

FIGURE 2. Channel flow scaling layer width distribution (a) inner-normalized and (b) as normalized by y. Data are from Hoyas & Jimenez (2006), Pirozzoli (2014), Lee & Moser (2015), Yamamoto & Tsuji (2018), Kaneda & Yamamoto (2021), and Hoyas et al. (2022).

the turbulent motions responsible for wall-normal momentum transport. The empirical estimation of ϕ_c as $\delta^+ \to \infty$ is the focus of Section 5, below.

3. Similarity solutions and layer hierarchy properties

3.1. *Similarity solutions for U^+ and T^+*

The condition in Eq. (2.5) closes the mean momentum equation, and the mean vorticity equation can be used to develop an integrable relation for either U^+ or T^+ on the $\phi = \phi_c$ part of the layer hierarchy. This results in

$$U^+(y^+) = \phi_c^2 \ln(y^+ - C_1) + C_2 y^+ + C_3, \tag{3.1}$$

$$\frac{\mathrm{d}T^+}{\mathrm{d}y^+} = \frac{\phi_c^2}{(y^+ - C_1)^2} - \frac{1}{\delta^+}, \tag{3.2}$$

with a subsequent integration yielding

$$T^+(y^+) = C_4 - \frac{\phi_c^2}{(y^+ - C_1)} - \frac{y^+\phi_c^2}{(y_m^+ - C_1)^2}. \tag{3.3}$$

In these expressions, y_m^+ is the location of the T^+ maximum (T_m^+), and because Eq. (2.4) becomes more accurate with increasing δ^+, C_1 through C_4 along with ϕ_c in Eqs. (3.1) and (3.3) are predicted to asymptote to fixed values at sufficiently large δ^+. In this regard, from Eqs. (3.2) and (3.3) one can show that

$$y_m^+ \to \phi_c\sqrt{\delta^+} \quad \text{as} \quad \delta^+ \to \infty \tag{3.4}$$

and

$$T_m^+ \to 1 \quad \text{as} \quad \delta^+ \to \infty, \tag{3.5}$$

both at a rate proportional to $1/\sqrt{\delta^+}$ (Klewicki et al. 2014). As is apparent, ϕ_c is ubiquitous in these solutions, which stems from its centrality to the self-similar structure admitted by Eq. (2.2).

3.2. *Layer hierarchy properties*

The scaling layer hierarchy exists on the domain where the TI profile is monotonically decreasing. Every point on this part of the profile uniquely defines a y^+ position and a layer of finite width $W^+(y^+)$. Since the invariant form given by Eq. (2.4) holds to leading order over each hierarchy layer, one can construct a discrete version on the $\phi = \phi_c$ domain where one layer abuts the next, such that

$$y_i + W_i = y_{i+1}. \tag{3.6}$$

Here, i and $i+1$ refer to the starting positions of adjacent discrete layers. This relation is convenient because, for example, when coupled with the asymptotic relation $W_i = y_i/\phi_c$, algebraic manipulation yields

$$y_i = \frac{\phi_c}{\phi_c + 1} y_{i+1}. \tag{3.7}$$

It is useful to consider the U^+ and T^+ increments across any given W^+ layer. On the $\phi = \phi_c$ part of the hierarchy, these are respectively given by

$$\Delta U^+|_{W_i^+} = \int_{y_1^+}^{y_i^+ + W_i^+} \frac{\mathrm{d}U^+}{\mathrm{d}y^+}\mathrm{d}y^+ = \phi_c^2 \ln\left(\frac{\phi_c + 1}{\phi_c}\right) \tag{3.8}$$

and

$$\Delta T^+|_{W_i^+} = \int_{y_i^+}^{y_i^+ + W_i^+} \frac{\mathrm{d}T^+}{\mathrm{d}y^+}\mathrm{d}y^+ = \frac{\phi_c^2}{y_i^+(\phi_c + 1)} - \frac{y_i^+}{\phi_c\delta^+}. \tag{3.9}$$

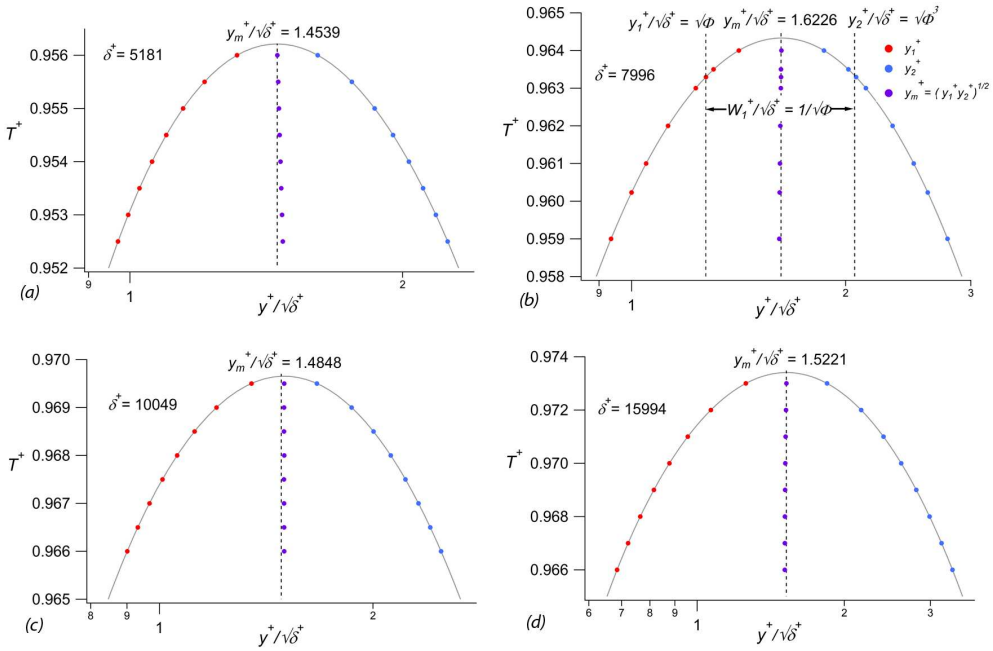

FIGURE 3. Behavior of Eq. (4.2) near y_m^+: (a) $\delta^+ = 5181$, (b) $\delta^+ = 7996$, (c) $\delta^+ = 10,049$, and (d) $\delta^+ = 15,994$. Data are from Lee & Moser (2015), Yamamoto & Tsuji (2018), Kaneda & Yamamoto (2021), and Hoyas et al. (2022).

4. Toward solving for ϕ_c

An inherent challenge to analytically solving for the asymptotic value of ϕ_c is that the similarity solutions in Eqs. (3.1) and (3.3) hold on an interior domain where the invariant form of Eq. (2.4) asymptotically exhibits exact self-similarity. In this case, self-similarity emerges precisely because an inertial interior region becomes insulated from any possible edge effects at the layer hierarchy periphery. Evaluating ϕ_c, however, requires an additional constraint (Klewicki 2021), such as a boundary condition, which is not available. On the other hand, because Eq. (2.5) closes Eq. (2.4), the U^+ and T^+ solutions are on an equal footing relative to an analytical evaluation of ϕ_c. As described below, the T^+ solution has some features that provide an additional constraint.

4.1. *Reynolds stress profile near* T_m^+

Reducing Eq. (3.3) under the condition $\delta^+ \to \infty$ yields

$$T^+(y^+) = 1 - \frac{\phi_c^2}{y^+} - \frac{y^+}{\delta^+}. \tag{4.1}$$

Noting that the T^+ solution holds from one hierarchy layer interior to y_m^+ to the centerline, the properties of Eq. (4.1) are now investigated in the vicinity of T_m^+. Specifically, if one considers positions $y_a^+ < y_m^+$ and $y_b^+ > y_m^+$, where $T_a^+ = T_b^+$, then from Eq. (4.1) it is simple to show that

$$\phi_c^2 = \frac{y_1^+ y_2^+}{\delta^+}, \tag{4.2}$$

or, equivalently, that $y_m^+ \equiv \phi_c/\sqrt{\delta^+}$ is equal to the geometric mean of y_a^+ and y_b^+. As shown in Figure 3(b), Klewicki (2021) used this relation to estimate ϕ_c at $\delta^+ = 7996$ (the largest Reynolds number channel DNS at the time) and found that the ensemble of the eight y_a^+, y_b^+ pairs depicted yield an average value for ϕ_c of 1.6195, with less than one viscous unit deviation from that value among the individual ensemble members. As discussed further in Section 5, deeper scrutiny reveals that this method exhibits sensitivities to subtle influences. Equation (4.1) is known to asymptotically hold, and in combination with the relations of the discrete scaling layer hierarchy under asymptotic conditions, it suggests a way to solve for ϕ_c. As discussed further below, however, this solution is not unique—for reasons that are currently only partially understood. Even so, it remains useful to describe the relevant arguments, since by doing so one gains insight into the T^+ solution structure.

4.2. *Exploiting the sole W^+ layer that spans the T^+ profile*

The rationale of Klewicki (2021) motivates further investigation into the constraint posed by considering the W^+ layer that begins at $y_1^+ = y_a^+$ and ends at $y_2^+ = y_b^+$. As shown in Figure 3(b), this layer spans the T^+ profile and by definition has zero ΔT^+. Use of Eq. (3.9) allows one to write an equation for the $\Delta T^+|_{W_1^+} = 0$ layer as

$$0 = \frac{\phi_c^2}{y_1^+(\phi_c + 1)} - \frac{y_1^+}{\phi_c \delta^+}. \tag{4.3}$$

Solving for y_1^+ results in

$$y_1^+ = \phi_c \sqrt{\frac{\phi_c \delta^+}{(\phi_c + 1)}}, \tag{4.4}$$

and recalling that $y_i^+ = \phi_c W_i^+$ yields

$$W_1^+ = \sqrt{\frac{\phi_c \delta^+}{(\phi_c + 1)}}. \tag{4.5}$$

Employing $y_2^+ = y_1^+ + W_1^+$ then gives

$$y_2^+ = (\phi_c + 1)\sqrt{\frac{\phi_c \delta^+}{(\phi_c + 1)}}. \tag{4.6}$$

Note also that for $y^+ < y_m^+$ the T^+ is monotonically increasing and for $y^+ > y_m^+$ it is monotonically decreasing (Figure 3). These features require that there be one and only one W^+ layer whose $\Delta T^+ = 0$ and that starts at $y_1^+ < y_m^+$ on the T^+ profile and ends at $y_2^+ > y_m^+$ on the T^+ profile. This property is known because W^+ is a monotonically increasing function of y^+; therefore, for layers originating at $y^+ < y_1^+$, the W^+ layer at that location will fall short of spanning the T^+ profile, and for layers originating at $y^+ > y_1^+$, the W^+ layer will overshoot the T^+ profile.

The idea is that the unique $\Delta T^+|_{W_1^+} = 0$ layer that spans Eq. (4.1) poses a constraint sufficient to analytically specify ϕ_c. That is, given that there is one and only one such W_1^+ layer, the argument is that there is a unique y_1^+ (expressed as a function of ϕ_c and δ^+) that satisfies Eq. (4.3); therefore, one only needs to find this apparently unique function. In this regard, the empirical evidence from Klewicki (2021) shown in Figure

3(b) indicates that $y_1^+ = \sqrt{\phi_c \delta^+}$ and thus $y_3^+ = \sqrt{\phi_c^3 \delta^+}$ constitute the end points of the $\Delta T^+|_{W_1^+} = 0$ layer to within a fraction of a viscous unit. These y_1^+ and y_2^+ values also satisfy all of the analytical conditions noted above.

Equation (4.3) can be rearranged to yield

$$\phi_c y_1^{+2} + y_1^{+2} = \phi_c^3 \delta^+. \tag{4.7}$$

By inserting $y_1^+ = \sqrt{\phi_c \delta^+}$ and dividing by ϕ_c, one obtains

$$\phi_c + 1 = \phi_c^2, \tag{4.8}$$

which has the golden ratio, $\Phi = (1+\sqrt{5})/2 \simeq 1.618034$, as its positive root solution. The above analysis leads to $\phi_c \to \Phi$ as $\delta^+ \to \infty$, in support of the conjecture by Klewicki et al. (2014). This solution, however, is not unique, as one can easily show that an infinite family of other y_1^+ values (say, $y_1^+ = \phi_c^{2/5}\sqrt{\delta^+}$) also results in a mathematically viable solution. At present, it is not entirely clear why the solution of Eq. (4.8) is not unique. It seems likely, however, that this circumstance stems from the $\Delta T^+|_{W_1^+} = 0$ constraint being dependent on the similarity structure admitted by Eq. (2.4). Thus, an additional constraint—indicating, for example, that both ϕ_c and δ^+ in the expression for y_1^+ must have the same exponent—is needed to clarify the present ambiguity. In this regard, the issues associated with empirically estimating ϕ_c provide additional insights.

5. Empirically estimating ϕ_c

Numerous ways to estimate ϕ_c stem from its direct connection to the statement of dynamical similarity given by Eq. (2.5) and, as a consequence, its pervasive appearance in Eqs. (3.1) and (3.3). As described by Klewicki (2021), the best estimates derive from expressions that have the fewest number of unknown constants (fitting parameters). These best estimates include directly measuring the W^+ profile slope (Figure 2(a)) or, even better, the average value of the ratio y^+/W^+ on the $\phi = \phi_c$ portion of the layer hierarchy (Figure 2(b); Klewicki & Philip 2025). The computation of $W^+(y^+)$, however, involves the terms in Eq. (2.2) and, thus, is not accessible from physical experiments to the required accuracy. Beginning at modest δ^+, however, fitting data from physical experiments to Eq. (3.1) with the logarithmic offset, C_1, set to zero yields consistently well-behaved results (Figure 4(b)).

Regarding most of the estimation methods, a specification of the fitting domain is important for exposing the progression of ϕ_c toward its asymptotic value (Klewicki & Philip 2025). The present theory provides a means to do so by systematically locating the inertial sublayer. Mathematically, this is where the logarithmic behavior in U^+ stems from the linear increase in the T^+ profile curvature as quantified by W^+. The start of the inertial sublayer is clear, as it is where the VF term in Eq. (2.2) becomes subdominant (i.e., at $y^+ \simeq 2.6\sqrt{\delta^+}$) (Wei et al. 2005). The end of the inertial sublayer is sensitive to data accuracy relative to quantifying the T^+ profile curvature. It is therefore pragmatically defined to be where the constant term in Eq. (3.2) exceeds the nonlinear term by a fixed factor that reflects the capacity of, for example, a DNS to reliably quantify this curvature. For the DNS tested by Klewicki & Philip (2025), a factor of about $40\times$ is appropriate, corresponding to a T^+ curvature of about 10^{-8}. This criterion locates the outer edge near $y^+ = 10.25\sqrt{\delta^+}$, which thus moves to smaller y/δ values with increasing δ^+.

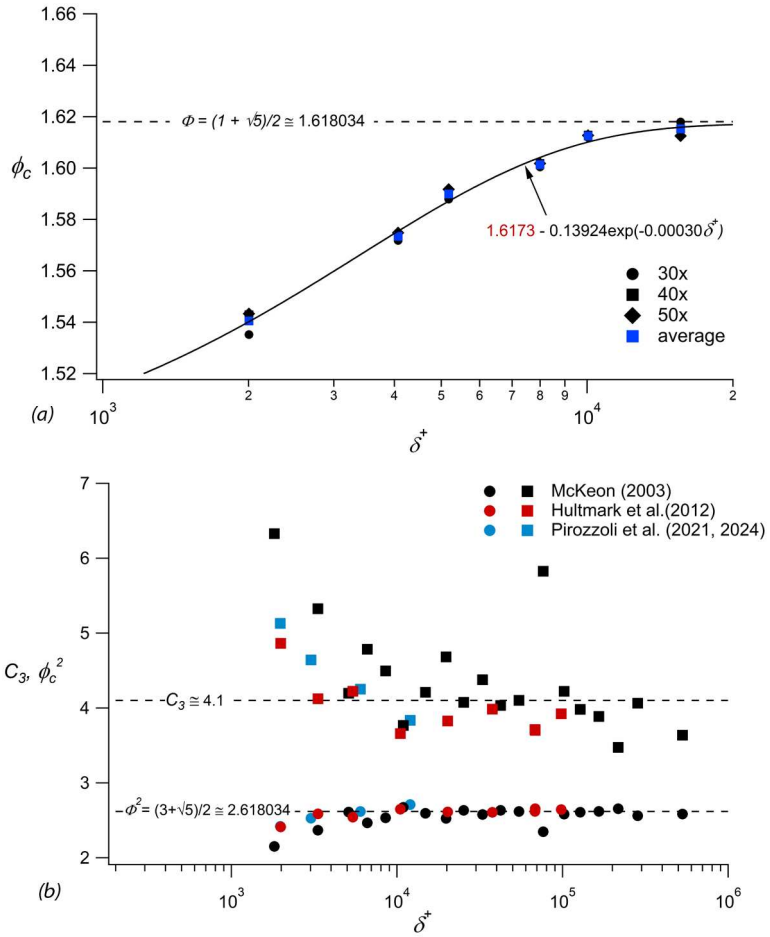

FIGURE 4. Empirical estimates of ϕ_c. (a) Average value of the inertial sublayer plateau for the channel flow data of Figure 2(b) using 30×, 40×, and 50× criteria for the outer edge of the inertial sublayer. (b) Pipe flow estimates of ϕ_c^2 and C_3 in Eq. (3.1). These data use a criterion between 50× and 70× in order to have at least 15 data points in the curve fit. Data are from McKeon (2003), Hultmark et al. (2012), and Pirozzoli (2024).

The results in Figure 4 reflect the dominant empirical finding that ϕ_c attains an essentially constant value of approximately 1.62 (i.e., very close to $\phi_c = \Phi$) for $\delta^+ > 10,000$. The previously described method involving Eq. (4.2), however, exhibits greater variation. These variations connect to a number of issues—including those associated with the accuracy and sensitivity of DNS realizations. As shown in Figure 3, the variation of y_m^+ with increasing δ^+ does not exhibit a clear trend toward a limiting value. Furthermore, the properties of the T^+ solution in the vicinity of T_m^+ exhibit inconsistencies with the other estimates for ϕ_c. That is, while Eq. (4.2) seems to hold reasonably well, indicating that the shape of the profile is consistent with the theory, the shape of the profile and the location of T_m^+ are apparently very delicately determined. For example, the $\delta^+ = 7996$ profile shows excellent agreement between y_m^+ and the spread of the T_m^+ profile (as assessed by the $\Delta T^+|_{W_1^+} = 0$ condition), as well as with the W^+ values computed from the $\mathrm{d}^2U^+/\mathrm{d}y^{+2}$ profile (i.e, $W^+ = (-\mathrm{d}^2U^+/\mathrm{d}y^{+2})^{-1/2}$, Klewicki (2021)).

The other profiles, however, show poorer agreement. For the $\delta^+ = 5181$ flow, this may in part be a low Reynolds number effect. It seems relevant to note that both the $\delta^+ = 5181$ and $\delta^+ = 10,049$ DNS have significantly larger Δy^+ grid spacings (about a factor of five larger) in the vicinity of y_m^+ than either the $\delta^+ = 7996$ or the $\delta^+ = 15994$ DNS. Thus, sufficient spatial resolution in this region is likely to be important for capturing the T^+ profile curvature. Lastly, the changes in the profile with δ^+ inherently produce sensitivities that may also be compounded by uncertainties owing to incomplete statistical convergence. For example, for the $\delta^+ = 15,994$ DNS, $y_m^+ = 1.5221\sqrt{\delta^+}$. The value of T^+ at $y^+ = 1.618\sqrt{\delta^+}$, however, varies in this flow from T_m^+ by only 0.0041%. Thus, the flattening of the profile inherent to $\delta^+ \to \infty$ presents additional challenges.

6. Summary

Analytical treatments exploiting the self-similar structure admitted by the mean dynamical equation in turbulent pipe and channel flows rationally lead to the solution $\phi_c = \Phi$ as $\delta^+ \to \infty$. This analysis leverages the unique location, $y^+ = y_1^+$, where a single W^+ layer on the scaling layer hierarchy spans the peak region of the T^+ profile such that $\Delta T^+ = 0$. The solution $\phi_c = \Phi$ is not, however, unique, even though it is unequivocally true that there is one and only one spanning W^+ layer. The reason for the non-uniqueness of the $\phi_c = \Phi$ solution may be that all the relations used by the analysis arise (either explicitly or implicitly) from the underlying self-similar structure. A sufficient further constraint would be to show that in the expression for y_1^+ both ϕ_c and δ^+ must scale with the same exponent. This would uniquely result in the $\phi_c = \Phi$ solution. Another way would be to identify a rigorous constraint that is external to the scaling layer hierarchy.

The accurate empirical determination of ϕ_c was recently advanced by precisely locating the start and end points of the inertial sublayer (Klewicki & Philip 2025). When these end points are used to define the data-fitting domain, the vast majority of estimates indicate that $\phi_c \to 1.59$–1.63 as δ^+ becomes large. A close examination of the T^+ solution in the vicinity of T_m^+ suggests that the precise shape and position of this profile are sensitive spatial resolution, and with increasing δ^+ the properties of this profile are increasingly susceptible to uncertainties (e.g., inadequate statistical convergence) and, thus, are difficult to discern owing to the flattening of the profile near T_m^+.

Acknowledgments

The support of ONR to CTR under grant N000142312833 is gratefully acknowledged. The author thanks Jonah Massey for his insightful comments associated with the review of this brief and the clarifying discussions with the PhD students in the ME 406 subject during the summer of 2025.

REFERENCES

Fife, P., Klewicki, J. & Wei, T. 2009 Time averaging in turbulence settings may reveal an infinite hierarchy of length scales. *J. Discrete Contin. Dyn. Syst. A* **24**, 781–807.

Hoyas, S. & Kraheberger, J. 2006 Scaling the velocity fluctuations in turbulent channels up to $\mathrm{Re}_\tau = 2003$. *Phys. Fluids* **18**, 011702.

Hoyas, S., Oberlack, M., Alcantara-Avila, F., Kraheberger, S. & Laux, J. 2022 Wall turbulence at high friction Reynolds numbers. *Phys. Rev. Fluids* **7**, 014602.

Hultmark, M., Vallikivi, J., Bailey, S. & Smits, A. 2012 Turbulent pipe flow at extreme Reynolds numbers. *Phys. Rev. Lett.* **108**, 094501.

Kaneda, Y. & Yamamoto, Y. 2021 Velocity gradient statistics in turbulent shear flow: an extension of Kolmogorov's local equilibrium theory. *J. Fluid Mech.* **929**, A13.

Klewicki, J. 2021 Properties of turbulent channel flow similarity solutions. *J. Fluid Mech.* **915**, A39.

Klewicki, J., Fife, P. & Wei, T. 2009 On the logarithmic mean profile. *J. Fluid Mech.* **638**, 73–93.

Klewicki, J., Fife, P. & Wei, T. 2014 Self-similarity in the inertial region of wall turbulence. *Phys. Rev. E* **90**, 063015.

Klewicki, J. & Philip, J. 2025 On the inertial sublayer of the mean velocity profile in turbulent channel and pipe flows. *Prog. Turb. XI.* In press.

Lee, M. & Moser, R. 2015 Direct numerical simulation of turbulent channel flow up to $\mathrm{Re}_\tau \sim 5200$. *J. Fluid Mech.* **774**, 395–415.

McKeon, B.J. 2003 High Reynolds number turbulent pipe flow. PhD Dissertation, Princeton University, Princeton, NJ.

Pirozzoli, S. 2014 Revisiting the mixing-length hypothesis in the outer part of turbulent wall layers: mean flow and wall friction. *J. Fluid Mech.* **745**, 378–417.

Pirozzoli, S. 2024 On the streamwise velocity variance in the near-wall region of turbulent flows. *J. Fluid Mech.* **989**, A5.

Wei, T., Fife, P., Klewicki, J. & McMurtry, P. 2005 Properties of the mean momentum balance in turbulent boundary layer, pipe and channel flows. *J. Fluid Mech.* **522**, 303–327.

Yamamoto, Y. & Tsuji, Y. 2018 Numerical evidence of logarithmic regions in channel flow at $\mathrm{Re}_\tau = 8000$. *Phys. Rev. Fluids* **3**, 012602(R).